Time Resolved Single Dopant Charge Dynamics in Silicon

M. Rashidi[1,2*], J. Burgess[3,4], M. Taucer[1,2], R. Achal[1], J. L. Pitters[2],
S. Loth[3,4], and R. A. Wolkow[1,2]

[1]Department of Physics, University of Alberta, Edmonton, Alberta, T6G 2J1, Canada.

[2]National Institute for Nanotechnology, National Research Council of Canada, Edmonton, Alberta, T6G 2M9, Canada.

[3]Max Planck Institute for the Structure and Dynamics of Matter, 22761 Hamburg, Germany.

[4] Max Planck Institute for Solid State Research, 70569 Stuttgart, Germany.

*Correspondence to:rashidi@ualberta.ca

As the ultimate miniaturization of semiconductor devices approaches, it is imperative that the effects of single dopants be clarified. Beyond providing insight into function and limitations of conventional devices, such information enables identification of new device concepts. Atomically resolved, electronic pump-probe scanning tunneling microscopy permits unprecedented, quantitative measurement of time-resolved single dopant ionization dynamics. Tunneling through the surface dangling bond makes feasible what would otherwise be too weak a signal to observe. We introduce a time-resolved scanning-tunneling-spectroscopy method whereby current measurements are made before the system of study relaxes or adjusts to accommodate an applied field. Distinct ionization and neutralization rates of a single dopant are measured and the physical process controlling those are identified.

Understanding the fundamental properties of individual dopants locally coupled to electronic transport in semiconductors is the focus of much current research (*1*). This area of enquiry holds promise for new semiconductor device applications at the ultimate level of miniaturization, as well as for utilization of the quantum properties of individual impurities (*2*). Scanning tunneling microscopy (STM) has enabled significant progress in this field, including observation of the influence of single dopants on the local density of states (LDOS) (*3–6*) and local magnetic properties (*7, 8*) of the host semiconductor. Measurements on GaAs have shown slow dopant dynamics can be observed locally with millisecond timescale STM (*9*). Dynamics must exist on much faster time scales as well, but have not yet been observed using STM. Time-resolved STM (TR-STM), pioneered by Nunes and Freeman (*10*), has recently seen a resurgence of interest (*11–15*) following the application of a simplified all-electronic technique to the measurement of spin dynamics in adatoms (*16*). Thus far, this method has only been applied to other magnetic adatom systems (*12*) and atomically assembled nanomagnets (*15*).
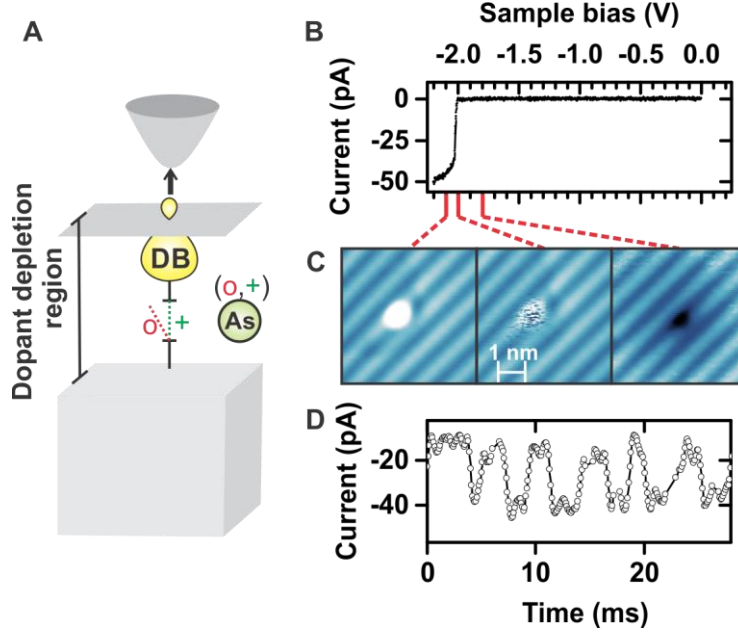
Fig. 1. Characteristic spectroscopic behavior of DBs on Si samples heated to 1250°C. (A) Simple diagram of the system of study representing the dopant as an on and off switch for the electron conduction from the bulk CB to the DB through the dopant deletion region as it changes from ionized to neutral. (B) Constant-height filled-state STS measured over a DB. (C) Constant-current STM images of the DB beyond (-2.1 V), at (-1.8 V) and before the critical voltage range (-2.0 V) at left, right, and center respectively. (D) Current time-trace at the critical voltage (-2.01V) exhibiting telegraph noise behavior at millisecond timescales.

Here, we measure single electron charge dynamics of individual subsurface dopants with time-resolution well beyond the limitations of conventional STM. By heating an otherwise degenerately doped silicon crystal to 1250°C, we induce a dopant depletion layer at the surface, leaving a low concentration of isolated dopants close to the surface that are only weakly coupled to the degenerately doped bulk silicon (*17*). Ionization of an arsenic dopant in the electric field of the tip opens a conductance channel from the conduction band (CB) to the tip via a surface dangling bond (DB), allowing transient switching analogous to a single atom gated transistor: the bulk acts as the source, the DB (strongly coupled to the tip) is the drain, and the dopant is the gate (Fig. 1 A). A combination of fast real-time acquisition and pump-probe techniques amplification enables temporal mapping of the local dopant dynamics from nanoseconds to seconds.

Scanning tunneling spectra (STS) of DBs on samples with the dopant depletion region are correlated with a sharp current onset (Fig. 1B) at a critical filled-state bias voltage (*18*). At sample biases less negative than the critical voltage (right panel in Fig. 1C), as a result of a weak supply of current from bulk to DB, the DB appears dark with a spatially extended halo, indicating an, on average, positively charged DB. Past the transition (left panel in Fig. 1C), the DB appears bright, indicating drastic increase in the supply of current from bulk to DB. In the critical voltage range (middle panel in Fig. 1C), the DB appears streaky in STM images. It
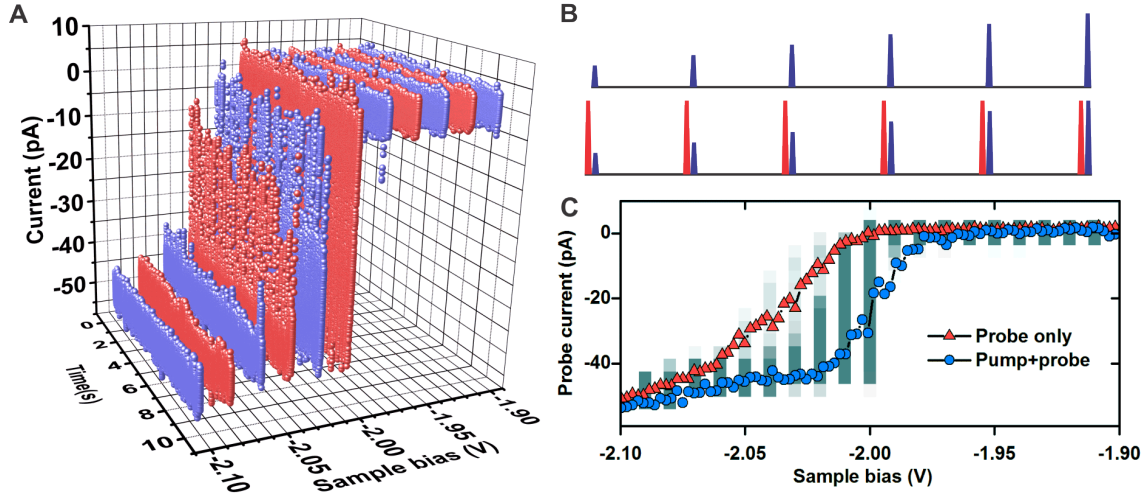
Fig. 2. Time-resolved scanning tunneling spectroscopy. (A) Current-time traces in the critical bias range in Fig. 1B, acquired with the maximum sampling rate of the STM controller (~10 kHz). Alternating colors are used for better visualization. (B) Schematic of TR-STS setup: Tunneling current is measured from a series of varying-amplitude probe-pulses with and without a preceding pump pulse (C) TR-STS with 1 μs probe pulses with (blue circles) and without (red triangles) a preceding 1 μs pump pulse. The DC bias voltage is set at -1.80 V. The amplitude of the pump pulse is 0.40 V and that of the probe pulse is swept from 50 to 400 mV. The relative delay between the pump and the probe pulse is 10 ns. The green color-map bars in the background are the projection of the current-time trace histograms in (A) with the intensity representing the amplitude of the time integrated signal. The observed hysteresis in TR-STS overlaps the bias range over which the system is bistable.

exhibits telegraph noise, stochastic switching between low conductance (LC) and high conductance (HC) states at millisecond timescales (Fig. 1D and 2A), similar in appearance to DB charge state fluctuations previously identified near Si DBs while using positive sample bias voltages(*19*). Since the observed switching rates are much slower than the rate of electrons passing through the DB (tunneling current of ~40 pA), these transitions cannot be caused by the charge fluctuation of the DB itself, indicating that stochastic switching of a nearby charge trap gates the current through the DB. This suggests the sharp current onset in Fig. 1 also corresponds to a dopant ionization, gating the conduction path from the bulk to the DB (Fig. 1A). These rates are at the limit of the STM's current preamplifier, making it impossible to see if the fluctuations extend beyond this slow timescale.

By means of all-electronic pump-probe STM, we show that dynamics exist beyond those visible through standard STM techniques. Figure 2B displays a schematic of time-resolved STS (TR-STS). The system properties are probed by a pulse train. On each probe cycle a preceding pump pulse disturbs the system by transiently pulsing the bias above the sharp transition threshold. The delay between pump and probe is fixed such that the pulses do not overlap. The DC bias is set as less negative than the critical voltage range, permitting the system to fully relax between pulse pairs. Thus the transient state immediately resulting from the pump is interrogated by the probe, and a transient I(V) curve may be measured by sweeping the probe pulse amplitude. As shown in Fig. 2C, the TR-STS of the DB exhibits hysteresis.
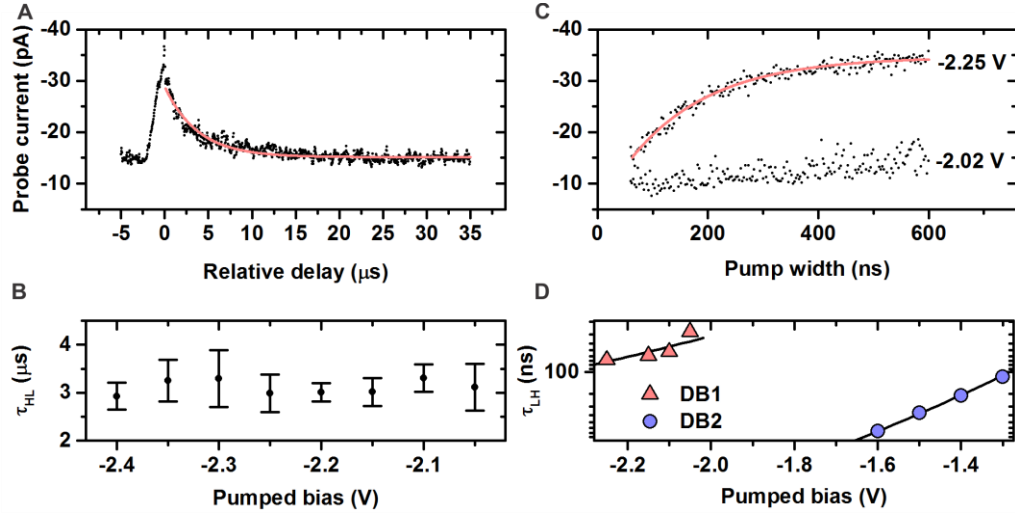
Fig. 3. TR-STM measurements of τ_{HL} and τ_{LH}. (A) τ_{HL} measurement from a 1 μs width probe pulse with a 1 μs width preceding pump pulse at different relative delays. The probe (pump) amplitude is 0.21 V (0.40 V). With the DC offset of -1.80 V, the probe and pump pulses are at -2.01 V and -2.20 V, respectively. (B) Measured τ_{HL} for different pump amplitudes shows that the time constant is independent of the pump bias. (C) τ_{HL} measurements at different bias voltage. The DC offset is -1.80 V and the probe width and relative delay is 1 μs and 10 ns, respectively. Red curves in (A) and (C) are the exponential fits. (D) τ_{LH} at different bias voltages for the DB in Fig. 1 (denoted here as DB1) and for DB2 which is fully described in the supplementary material. Solid lines are the fits using Equation 2.

We measure the relaxation from the high conductance state to the low conductance state (τ_{HL}) using a conventional pump-probe measurement. Here the pump and probe pulse amplitudes are fixed, while the delay is swept (See the supplementary material). Figure 3A shows a decay in the pump-probe measurement of τ_{HL}, acquired by a standard pump-probe approach, using fixed pulse amplitudes but varying the delay between the pump and the probe pulses. The pump-probe curve can be fit with a single exponential decay function. To check for dynamics at other time scales which are triggered at different critical voltages, τ_{HL} is measured while the pump amplitude is swept (Fig. 3B). Between the pump voltage of -2.4V and -2.05V we find an approximately constant lifetime of $\tau_{HL}=3.1\pm0.1$ μs, indicating that there is only one process active in this bias range.

To probe the excitation dynamics, we perform pump-probe experiment varying the pump length rather than the pump probe delay. Probing at a fixed delay following a variable pump length enables measurement of the probability that the system transitioned to the high conductance state during the pump. The DC bias is set such that the system returns to the low conductance condition in the intervening time between pump-probe pairs. Figure 3C displays τ_{LH} as a function of pumping bias. τ_{LH} at different pump bias voltages for the DB in Fig. 1 and the DB presented in the supplementary material are displayed in Fig. 3D. For short pump widths, the system stays in the low conductance state. Increasing the pump width, it exponentially transitions to the high conductance state. The time constant of the exponential increase gives the time
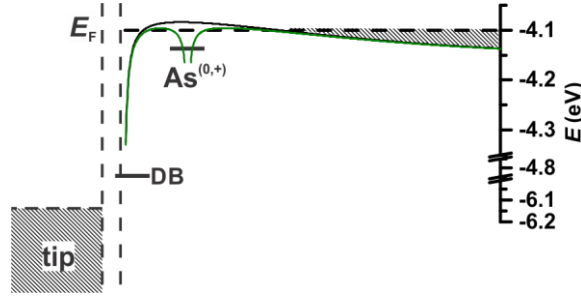
Fig 4. Schematic of the CB edge with (green curve) and without (black curve) an ionized dopant in the vicinity of a DB.

needed to pump the system, τ_{LH}. Unlike τ_{HL}, τ_{LH} shows a strong dependence on the pump amplitude.

The results in Fig. 3C and D can be understood in terms of tunnel ionization of a neutral dopant in the field of the STM tip and of other ionized dopants. The field due to the STM tip, and consequent tip induced band bending (TIBB), is linear in bias to a first approximation and crosses zero at the flat band condition. Furthermore, we expect that if a dopant is at the point of field ionization then dopants nearer to the surface, where the field is higher, will already be ionized, adding to the ionizing field experienced by the dopant in question. The field strength experienced by the dopant then approximated by

$$F = \kappa \left| V_S + V_{CPD} \right| + \frac{ed_{As}N_D^{surf}}{2\epsilon},$$ (1)

where κ is a constant of proportionality related to TIBB, V_{CPD} is the contact potential difference, defined as the difference between work functions, $\varphi_{tip} - \varphi_{Si}$, d_{As} is the depth of the arsenic dopant, $N_D^{(Surf)}$ is the dopant density at the surface, and ε is the dielectric constant of silicon. The ionization rate as a function of field strength can be analytically expressed in the case of the hydrogen atom (*20*). Adapted to the case of a hydrogen-like arsenic dopant, it reads

$$\Gamma_E\left(F\right) = \frac{128\pi\varepsilon E_{As}^3}{\hbar e^3 F} \exp\left(\frac{-32\pi\varepsilon E_{As}^2}{3e^3 F}\right),$$

(2)

where E_{As} is the binding energy of the As dopant. The exponential dependence of the ionization rate on the inverse field strength accounts for the sharp transition in the dopant charge state as the sample bias crosses the critical voltage. Equations (1) and (2) are used to fit the experimental data in Fig. 3D, with κ and d_{As} as free parameters. The resulting fits are consistent with dopant depths of approximately 1.4 nm. In both cases, the model correctly shows that the ionization rate of the As dopants depend sensitively on the tip field (*20*), given by the potential gradient at the dopant position, including the effect of TIBB. Conversely, over a small voltage range, the rate of electron supply to the dopant is, to a first approximation, independent of the tip field.

The detection mechanism of the donor dynamics, the gating effect of the donor on conduction from bulk to the DB at the surface, is also captured in this model. As a result of the dopant depletion region the degenerately doped bulk does not extend to the surface and the CB edge presents a potential barrier separating the carriers in the degenerately doped region from the surface and DB (Fig. 4). This potential barrier accounts for the weak supply of electrons from the

5

bulk to the DB for sample biases less negative than the critical voltage. As the critical voltage is crossed, we associate the sudden change in the supply rate of the DB with dopant ionization in the tip field, as similar systems have been previously (*3–6*). The electrostatic effect of the ionized dopant significantly reduces the potential barrier which can lead to an increase in the conductivity from bulk to surface. This same scenario describes the standard I(V) STS measurements through the DB. For voltages below the current onset, the ionization rate of the donor is much smaller than its supply rate resulting in a neutral charge state on average. As the tip field increases, the ionization rate rapidly overtakes the supply rate, leading to a positive charge of the As donor on average. Only in the narrow transition region between these two extremes is it possible to observe the ionization dynamics of nearby dopants.

This model permits a robust description of the dynamics observed and demonstrates that the sharp tunneling current features in stem from the gating influence and ionization thresholds of nearby dopants. More importantly, in conjunction with the ability of TR-STM to identify discrete voltage thresholds triggering separate time scales of dynamics, the model permits the disentanglement of the influence of multiple dopants. Here we analyze a case with two dopants, one slow with a strong effect on conduction to the DB, and one fast with a weaker influence as an example that captures a broad range of behavior. However, the range of variability in numbers and interactions of nearby dopants readily explains the wide range of critical voltages and sets of multiple current steps seen in DC measurements of DBs (*18*).

The Si surface DB is a convenient and powerful probe for dynamics of local dopants that may be used with TR-STM to understand complex environments. The combined technique and system has great potential in exploring the effects of sparse dopants in transistors, and in prototyping novel devices based on interacting or isolated dopants.

References:

1.   P. M. Koenraad, M. E. Flatté, Single dopants in semiconductors. *Nat. Mater.* **10**, 91–100 (2011).

2.   A. Morello *et al.*, Single-shot readout of an electron spin in silicon. *Nature*. **467**, 687–691 (2010).

3.   J. A. Mol, J. Salfi, J. A. Miwa, M. Y. Simmons, S. Rogge, Interplay between quantum confinement and dielectric mismatch for ultrashallow dopants. *Phys. Rev. B*. **87**, 1–7 (2013).

4.   F. Marczinowski *et al.*, Local Electronic Structure near Mn Acceptors in InAs: Surface-Induced Symmetry Breaking and Coupling to Host States. *Phys. Rev. Lett.* **99**, 157202 (2007).

5.   J. Salfi *et al.*, Spatially resolving valley quantum interference of a donor in silicon. *Nat. Mater.* **13**, 605–10 (2014).

6.   B. Voisin, J. Salfi, J. Bocquel, R. Rahman, S. Rogge, Spatially resolved resonant tunneling on single atoms in silicon. *J. Phys. Condens. Matter*. **27**, 154203 (2015).

7.   A. a Khajetoorians *et al.*, Detecting excitation and magnetization of individual dopants in a semiconductor. *Nature*. **467**, 1084–1087 (2010).

8.   D. Kitchen, A. Richardella, J. M. Tang, M. E. Flatté, A. Yazdani, Atom-by-atom substitution of Mn in GaAs and visualization of their hole-mediated interactions. *Nature*. **442**, 436–439 (2006).

9.   K. Teichmann *et al.*, Bistable charge configuration of donor systems near the GaAs(110) surfaces. *Nano Lett.* **11**, 3538–42 (2011).

10.   G. Nunes, M. R. Freeman, Picosecond resolution in scanning tunneling microscopy. *Science*. **262**, 1029–1032 (1993).

11.   C. Grosse, M. Etzkorn, K. Kuhnke, S. Loth, K. Kern, Quantitative mapping of fast voltage pulses in tunnel junctions by plasmonic luminescence. *Appl. Phys. Lett.* **103**, 183108 (2013).

12.   S. Loth, S. Baumann, C. P. Lutz, D. M. Eigler, A. J. Heinrich, Bistability in atomic-scale antiferromagnets. *Science*. **335**, 196–9 (2012).

13.   I. Moult, M. Herve, Y. Pennec, Ultrafast spectroscopy with a scanning tunneling microscope. *Appl. Phys. Lett.* **98**, 233103 (2011).

14.   C. Saunus, J. Raphael Bindel, M. Pratzer, M. Morgenstern, Versatile scanning tunneling microscopy with 120 ps time resolution. *Appl. Phys. Lett.* **102**, 051601 (2013).

15.   S. Yan, D.-J. Choi, J. A. J. Burgess, S. Rolf-Pissarczyk, S. Loth, Control of quantum magnets by atomic exchange bias. *Nat. Nanotechnol.* **10**, 40–45 (2014).

16.   S. Loth, M. Etzkorn, C. P. Lutz, D. M. Eigler, A. J. Heinrich, Measurement of fast electron spin relaxation times with atomic resolution. *Science*. **329**, 1628–30 (2010).

17.   J. L. Pitters, P. G. Piva, R. a. Wolkow, Dopant depletion in the near surface region of thermally prepared silicon (100) in UHV. *J. Vac. Sci. Technol. B*. **30**, 021806 (2012).

18.   H. Labidi *et al.*, Scanning tunneling spectroscopy reveals a silicon dangling bond charge state transition. *New J. Phys.* **17**, 073023 (2015).

19.   M. Taucer *et al.*, Single-Electron Dynamics of an Atomic Silicon Quantum Dot on the H-Si(001)-(2×1) Surface. *Phys. Rev. Lett.* **112**, 256801 (2014).

20.   L. Landau, E. Lifshitz, *Quantum Mechanics* (Pergamon, New York, 1965).

21.   M. Rezeq, J. Pitters, R. Wolkow, Tungsten nanotip fabrication by spatially controlled field-assisted reaction with nitrogen. *J. Chem. Phys.* **124**, 204716 (2006).

22.   J. J. Boland, Scanning tunnelling microscopy of the interaction of hydrogen with silicon surfaces. *Adv. Phys.* **42**, 129–171 (1993).

23.   A. Hoffmann, M. T. Woodside, Signal-Pair Correlation Analysis of Single-Molecule Trajectories. *Angew. Chemie Int. Ed.* **50**, 12643–12646 (2011).

24.   R. M. Feenstra, Electrostatic potential for a hyperbolic probe tip near a semiconductor. *J. Vac. Sci. Technol. B*. **21**, 2080–2088 (2003).

Acknowledgments:

Supplementary Materials for

Time Resolved Single Dopant Charge Dynamics in Silicon

M. Rashidi[*], J. Burgess, M. Taucer, R. Achal, J. L. Pitters, S. Loth, and R. A. Wolkow

*correspondence to: rashidi@ualberta.ca

Materials and Methods

Methods

Measurements were performed using an Omicron LT-STM and Nanonis control system at a temperature of 4.5 K with a base pressure of 5×10^{-11} Torr. The STM is commercially equipped with radio frequency (RF) wiring with a bandwidth of ~500 MHz. The tungsten tips were chemically etched and cleaned and sharpened by electron beam heating followed by field ion microscopy (*21*). The samples were cleaved from a 3–4 mΩ.cm n-type arsenic doped Si(100) wafers (Virginia Semiconductor Inc.). They were degassed for several hours at 600°C and were cleaned by multiple flash annealing to approximately 1250°C then hydrogen-terminated near 330°C (*22*). The high temperature flash anneal leads depletion of dopants in a surface region 60 nm wide as measured by SIMS (*17*). $I(V)$ spectra were measured in constant-height mode and tip quality was checked by performing reference spectroscopy on bare silicon and bare dimer defects. Voltage pulses and gentle, controlled contacting of tip to sample was used to improve the tip quality for STM imaging and spectroscopy in-situ.

Time-resolved Scanning Tunneling Microscope Setup

As shown schematically in Fig. S1, cycles of voltage pulse pairs were generated by an arbitrary function generator (AFG), Tektronix AFG3252C, summed (Mini-Circuits ZFRSC-42-S+), and fed into the tip. The DC bias voltage was applied to and the tunneling current was collected through an Omicron preamplifier, which is connected to the sample. Two RF switches (Mini-Circuits ZX80-DR230-S+) connected to AFG output channels were used to either ground the tip during STM imaging and spectroscopy or connect the tip to the AFG during pump-probe measurements.
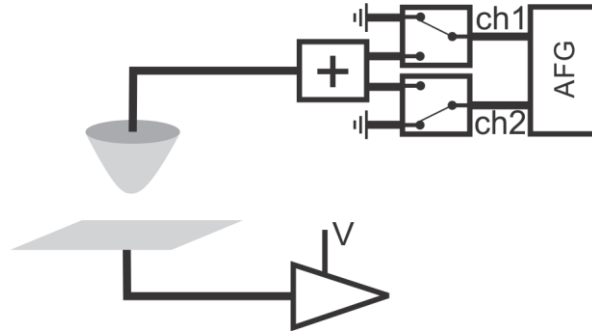

Fig. S 1 TR-STM setup.

The Auto-correlation signal measured on H:Si was used to monitor the quality of the pulses at the tunnel junction. Ringing is a common problem in this technique due to the imperfect impedance match between the tunnel junction and 50 Ω impedance of the rest of the setup (*11*). To dampen the ringing, 25 ns wide pulse edges were used throughout this work.
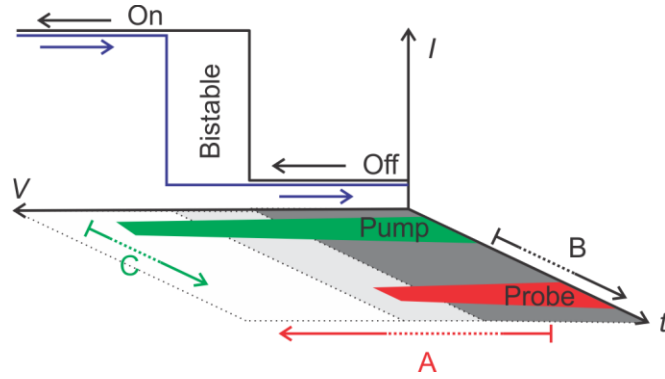
Fig. S 2 (A) TR-STS: tunneling current is measured from a series of varying-amplitude probe-pulses with and without a preceding pump pulse. (B) τ_{HL} measurement: a pump pulse is applied and a proceeding probe pulse at different relative delay checks the status of the system at a bistable sample bias. (C) τ_{LH} measurement: A pump pulse with varying width is applied and a proceeding probe pulse shortly after checks the status of the system at a bistable sample bias.

Time-Resolved Scanning Tunneling Spectroscopy

For measuring time-resolved scanning tunneling spectroscopy (TR-STS) as shown schematically in Fig. S2A, tunneling current, rather than resulting from a continuous DC bias, is instead produced by a series of short voltage pulses, denoted as probe pulses, at different amplitudes. Duty cycle, repetition rate, and total measuring time need to be adjusted to allow sufficient signal for the measurements. On the other hand, care must be taken to ensure that the system's state is not significantly changed during the time the pulse is on as well as to allow the system to return to its equilibrium state within the time when the pulse is off, in the case where it has been "pumped" to a different state. The state of the system at the time when it is probed can be set either by a DC offset, or by a preceding pulse, referred to as a pump pulse, with a very short or even zero relative delay between two pulses. The relative delay is defined as the time between the trailing edge of the pump pulse and the leading edge of the probe pulse.

Time Constant Measurement of Transition from High to Low Conductance State

As shown schematically in Fig. S2B, to measure the time constant of the transition from high to low conductance (τ_{HL}), the DC offset is set at a sample bias voltage where the system is in the low conductance state (LC). A pump pulse brings the system to the high conductance (HC) state and a subsequent probe pulse at different relative delays probes the status of the system at a sample bias at which bistability occurs. Within the relative delay time the applied bias is the DC offset, which has the effect of bringing the system to the LC state. At zero relative delay, the system is in the HC state. As the relative delay is increased, the system transitions to the LC state. The time constant of the exponential decay, is a measure of the characteristic time over which the system randomly transitions from the HC state to the LC state.

Time Constant Measurement of Transition from Low to High Conductance State

The schematic of time constant measurement for transition from low to high conductance state (τ_{LH}) is shown in Fig. S2C. A pump pulse with varying width is applied to bring the system to the HC state and a subsequent probe pulse shortly after checks the state of the system at a sample bias at which bistability occurs. In order to calculate the current from the probe pulse only, for each pump width, the signal is measured with a small amplitude probe pulse and the result is subtracted from the measured signal with the probe pulse at the bistable bias range. A DC bias offset is applied at sample biases more positive than the bistable bias range to bring the system to the LC condition in the intervening time between pump-probe pairs. For short pump width, the system stays "off" and the probe current is almost zero. By increasing the pump width the average probe current increases exponentially and reaches its maximum value. The time constant of the exponential increase gives the time needed to pump the system, τ_{LH}.

Since the current is almost zero at the DC offset, the measured tunneling current from the preamplifier comes almost exclusively from current during the time when the pulses are on. In order to obtain the actual current from the probe pulse, the measured current from the preamplifier is divided by the duty cycle of the pulse series and the current from the pump pulse is subtracted from that. The close match between this calculated current of the transient I(V) and the current obtained by DC I(V) at bias voltages outside the bistable region provides further evidence that the current comes predominantly from the pulses.

Signal Pair Analysis of Slow Transitions in the Bistable Energy Regime

The transition rates between the HC and LC states were calculated using a form of signal-pair analysis (*23*). The current-traces were placed in histograms and the HC and LC states were fit with Gaussian functions similar to (*19*). Regions within each state were selected to minimize the overlap with other states, and correlations between pairs of regions were calculated based on a linear pathway. The transition rates were determined directly from the fit of derived correlation functions (*23*) to these generated correlation data.
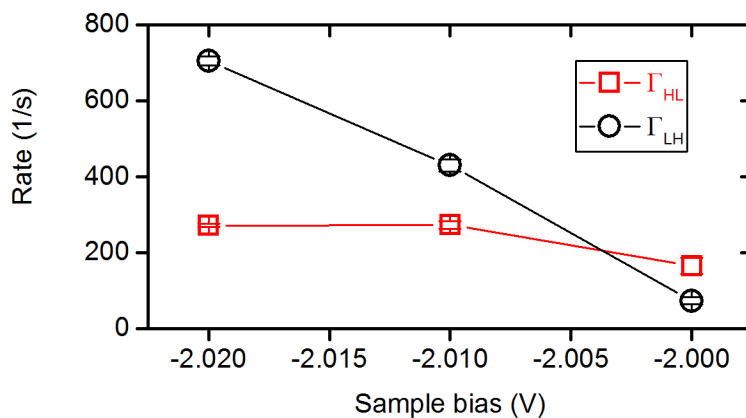

Fig. S 3 Rates from telegraph data in the bistable energy regime, calculated by signal pair analysis method.

Additional Example: TR-STM on a slow switching DB

The spectroscopic characteristics of dangling bonds (DB) on samples prepared by heating to 1250°C diverges because of the variation in their local environment (*18*). Therefore, we show another example here to show that while the measured rates among different DBs are quantitatively different, different DBs qualitatively exhibit similar behavior. We present a DB (denoted as DB2 in Fig. 3D of the main manuscript) with the sharp current onset at ~ -1.15 V and with the transitions in the bistable energy regime in the range of seconds. This is very different from the DB studied in the main manuscript, which exhibits the current onset at ~ -2.00 V and transition rates in the bistable energy regime of a few hundred hertz. The slow transitions at this DB lead to hysteresis in forward and backward I(V) sweeps (Fig. S4) when the total sweep time is less than a few seconds. Only for relatively slow measurements (sweep time of ~ 6.5 s) does the hysteresis loop vanish.
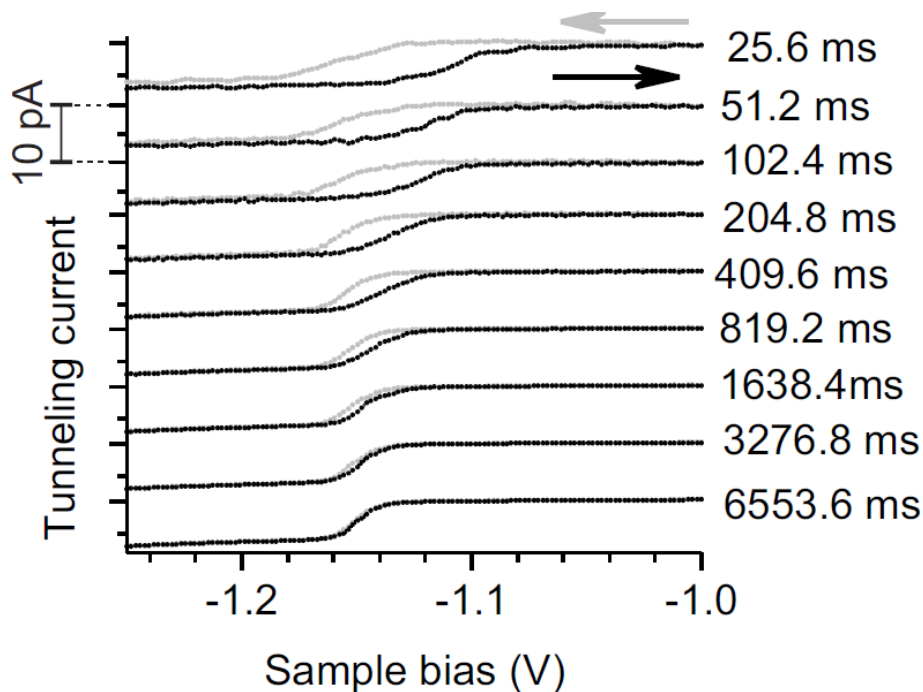

Fig. S 4 Forward (-1.2 V to -1.0 V) and reverse bias spectroscopy sweeps in the case of a DB with slow time dynamics reveals conductance hysteresis. The I(V) curves are the averages of 100 sweeps at different total sweep times indicated on the side of each curve. The hysteresis loop closes for sweep times around 6.5 s, indicating dynamics in the range of hertz at the transition bias.

Figure S5 displays TR-STS on this DB. The TR-STS shows a wider hysteresis loop than any of the conventional STS sweeps, in agreement with the trend of widening of the hysteresis loop for faster I(V) sweeps observed in Fig. S4. The time-resolved spectra measured with and without the pump pulse are analogous to forward and reverse sweeps of the conventional spectra shown in Fig. S4, respectively.
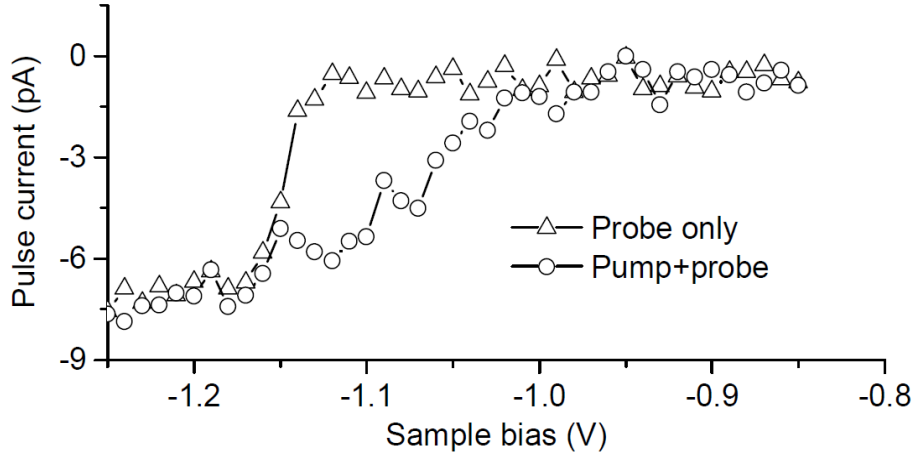

Fig. S 5 TR-STS on the DB in Fig. S4. Current from a 1 μs width probe pulse with and without a 10 μs width preceding pump pulse. The delay from the trailing edge of the pump pulse to the leading edge of the probe pulse is 10 ns and the DC bias voltage is set at -0.80 V. The amplitude of the pump pulse is 0.60 V and that of the probe pulse is swept from 50 to 450 mV. Since the polarity of both pulses is negative, the pumped bias is -1.40 V and the probe sweeps the bias range of -0.85 to -1.25 V.
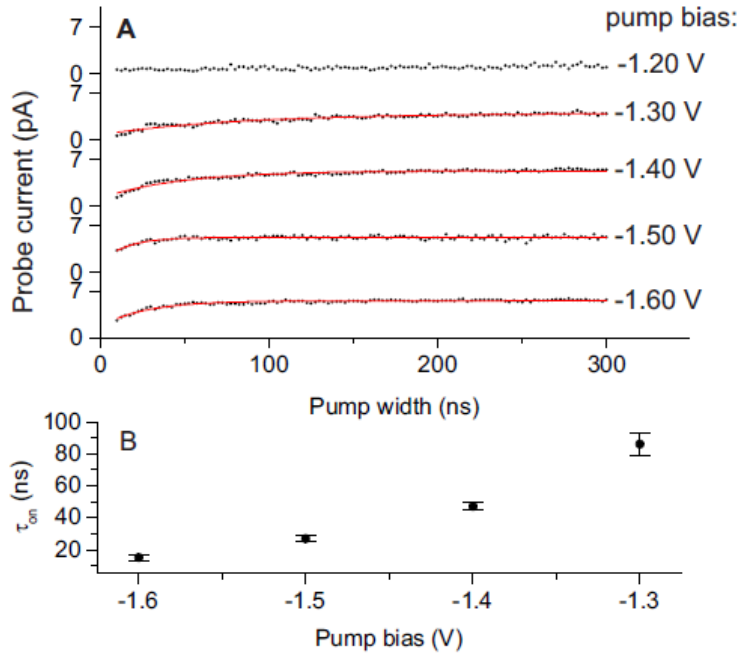

Fig. S 6. (A) TR-STM measurement of τ_{LH} at different pump bias on the DB in Fig. S4. The DC offset is -0.80 V. The probe width and relative delay is 1 μs and 10 ns, respectively. Red curves are exponential fits. (B) τ_{LH} vs. pumped bias.

15

Theoretical Treatment of Tunnel Ionization of Neutral As Donors

Donors are ionized in the field of the tip. The bound electron tunnels through a triangular barrier formed by the confining potential of the host donor and the tilted potential of the field, as shown in Fig. S7A. Ionization rate is a function of field strength, which can be derived analytically for the Hydrogen atom,

$$\Gamma_E\left(F\right) = \frac{4m^3 e^9}{\hbar^7 F} \exp\left[\frac{-2m^2 e^5}{3\hbar^4 F}\right].$$

To treat the case of an arsenic donor in silicon, we adapt this relation and express it in terms of the binding energy, as

$$\Gamma_E\left(F\right) = \frac{128\pi\varepsilon E_{bind}}{\hbar e^3 F} \exp\left[\frac{-32\pi\varepsilon E_{bind}}{3e^3 F}\right],$$

as in equation (2) of the manuscript. The binding energy and dielectric constant in this equation are modified from the case of the hydrogen atom in vacuum to reflect the binding energy of the As donor and the dielectric constant of silicon. This form of the ionization rate as a function of field strength does not explicitly include the effective mass of the electron, instead using the known binding energy of 54 meV. This is done since the effective mass treatment of an electron donor in silicon underestimates the binding energy by a factor of nearly two. Since the binding energy plays a very important role in determining the rate of tunnel ionization, we choose to insist on this quantity in our treatment of donors.

Fig. S7(B) shows ionization as a function of field strength. The rate increases non-linearly, and within the fields that can be experienced by near-surface donors, we see that there is a dramatic change in the ionization rate from effectively zero, to much faster than the timescales that are accessible in STM experiments, shown as shaded regions in the inset of Fig. S7(B). The sharp transition studied in this paper is due to this rapid transition in rates as the field experienced by a donor increases.

As the sample bias becomes increasingly negative in an STM experiment, the tip has an increasing field effect on nearby donors (although the effect of contact potential must also be taken into account). The field eventually becomes large enough to ionize a donor, making it positively charged. As the field increases further, deeper donors may ionize. These deeper donors, however, experience an additional field due to the positive charge of already-ionized donors nearer to the surface. In a quasi-one dimensional approach, we can assume that when a given donor is near its ionization threshold, any donors nearer to the surface must already be ionized. The expected field, subject to the randomness of dopant locations, is given by the positive charge density that a donor sees on the surface side. We treat these donors as a uniformly distributed charge, resulting in the following expression for the field experienced by a donor at depth d_{As},

$$F_{don} = \frac{e d_{As} N_D^{surf}}{2\varepsilon},$$

which appears as the second term in Equation (1). This is the expected z-component of the field experienced by a donor near its critical field. In practice, it will vary due to the randomness of its environment, and will in general also have components in the x-y plane.
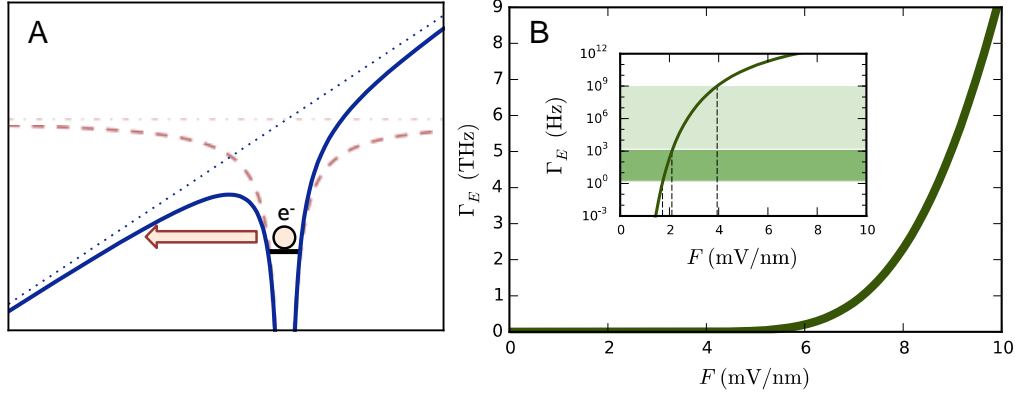

Fig. S 7 (A) The arsenic donor can be stripped of its bound electron through tunnel ionization in the presence of a field. (B) Ionization rate as a function of field strength. Inset shows a semi-logarithmic plot with the dark shaded region indicating the typical timescales for standard STM measurements. The lighter shaded region indicates the timescales that are accessible in TR-STM.